Investigating the use of virtual 4DCT from 4DMRI in gated carbon ion radiation therapy of abdominal tumors

Giorgia Meschini[a,*,1], **Alessandro Vai**[b,1], **Chiara Paganelli**[a], **Silvia Molinelli**[b], **Davide Maestri**[b], **Giulia Fontana**[b], **Andrea Pella**[b], **Viviana Vitolo**[b], **Francesca Valvo**[b], **Mario Ciocca**[b], **Guido Baroni**[a,b]

[a] Department of Electronics, Information and Bioengineering, Politecnico di Milano, Milano 20133, Italy
[b] Centro Nazionale di Adroterapia Oncologica, Pavia 27100, Italy

Received 28 February 2020; accepted 31 August 2020

Abstract

Purpose: *To generate virtual 4DCT from 4DMRI with field of view (FOV) extended to the entire involved patient anatomy, in order to evaluate its use in carbon ion radiation therapy (CIRT) of the abdominal site in a clinical scenario.*

Materials and methods: *The virtual 4DCT was generated by deforming a reference CT in order to (1) match the anatomy depicted in the 4DMRI within its FOV, by calculating deformation fields with deformable image registration to describe inter-fractional and breathing motion, and (2) obtain physically plausible deformation outside of the 4DMRI FOV, by propagating and modulating the previously obtained deformation fields. The implemented method was validated on a digital anthropomorphic phantom, for which a ground truth (GT) 4DCT was available. A CIRT treatment plan was optimized at the end-exhale reference CT and the RBE-weighted dose distribution was recalculated on both the virtual and GT 4DCTs. The method estimation error was quantified by comparing the virtual and GT 4DCTs and the corresponding recomputed doses. The method was then evaluated on 8 patients with pancreas or liver tumors treated with CIRT using respiratory gating at end-exhale. The clinical treatment plans adopted at the National Center for Oncological Hadrontherapy (CNAO, Pavia, Italy) were considered and the dose distribution was recomputed on all respiratory phases of the planning and virtual 4DCTs. By comparing the two datasets and the corresponding dose distributions, the geometrical and dosimetric impact of organ motion was assessed.*

Results: *For the phantom, the error outside of the 4DMRI FOV was up to 4.5 mm, but it remained sub-millimetric in correspondence to the target within the 4DMRI FOV. Although the impact of motion on the target $D_{95\%}$ resulted in variations ranging from 22% to 90% between the planned dose and the doses recomputed on the GT 4DCT phases, the corresponding estimation error was $\leq$2.2%. In the patient cases, the variation of the baseline tumor position between the planning and the virtual end-exhale CTs presented a median (interquartile range) value of 6.0 (4.9) mm. For baseline variations larger than 5 mm, the tumor $D_{95\%}$ variation between the plan and the dose recomputed on the end-exhale virtual CT resulted larger than 10%. Median variations higher than 10% in the target $D_{95\%}$ and gastro-intestinal OARs $D_{2\%}$ were quantified at the end-inhale, whereas close to the end-exhale phase, limited variations of relevant dose metrics were found for both tumor and OARs.*

Conclusions: *The negligible impact of the geometrical inaccuracy in the estimated anatomy outside of the 4DMRI FOV on the overall dosimetric accuracy suggests the feasibility of virtual 4DCT with extended FOV in CIRT of the abdominal site. In the analyzed patient group, inter-fractional variations such as baseline variation and breathing variability were quantified, demonstrating the method capability to support treatment planning in gated CIRT of the abdominal site.*

Keywords: Carbon ion therapy, Motion, Virtual 4DCT, 4DMRI

* Corresponding author: G. Meschini, Department of Electronics, Information and Bioengineering, Politecnico di Milano, Milano 20133, Italy.
E-mail: giorgia.meschini@polimi.it (G. Meschini).
[1] These authors contributed equally to this work.

Z Med Phys **32** (2022) 98–108
https://doi.org/10.1016/j.zemedi.2020.08.005
www.elsevier.com/locate/zemedi

1 Introduction

In particle therapy, the physical properties of protons and carbon ions are exploited to achieve highly conformal dose distributions with optimal target coverage and improved sparing to surrounding organs at risk (OARs) [1]. For carbon ion radiotherapy (CIRT), the high linear energy transfer (LET) radiation contributes to various biological advantages which concur to improved clinical outcome [2]. Encouraging results for liver tumors as well as favorable outcomes in pancreatic cancer demonstrated that CIRT represents a viable therapeutic option for abdominal tumors [3–6] and recently motivated prospective studies in this direction [7].

In this scenario however, organ motion of the abdominal site could have a severe impact on the dose distribution [8]. In addition to the risk of target miss, differences in tissue composition proximal to the target modify the particle range causing variations in dose deposition on the OARs along the beam path and target under coverage. Also, the use of pencil-beam scanning (PBS) technique suffers from interplay effects between particle delivery and organ motion [9–11], thus affecting treatment accuracy. Moreover for CIRT, absorbed dose variations translate in a non-linear way to relative biological effectiveness (RBE) weighted dose differences, thus degrading again homogeneity and conformity in target dose [12].

Organ motion should therefore be accurately accounted for, and several possible motion mitigation strategies have been proposed [8,13,14]. At the Italian National Center for Oncological Hadrontherapy (CNAO, Pavia, Italy), a combined approach for proton and carbon ion plan treatments of thoraco-abdominal tumors comprises mild abdominal compression, gating at the respiratory end-exhale phase ($\approx$1 s gating window) and layer rescanning [15]. Treatment planning is typically performed relying on a four-dimensional computed tomography (4DCT) image, which represents the patient's anatomo-pathological condition only within the time interval of the CT acquisition itself [16]. Extra information needs therefore to be acquired during the treatment course for capturing anatomo-pathological changes and respiratory pattern modifications which may alter the delivered dose distribution [17–19]. Although daily cone-beam CT (CBCT) acquisition should take into account respiratory motion [20,21], it is not currently used in the clinical routine as direct dose calculation on CBCT images is not recommended for Intensity Modulated Particle Therapy (IMPT) [22] due to their poor image quality [23]. Re-evaluative 4DCT scans during the treatment course are therefore currently acquired once a week to evaluate the impact of inter- and intra-fraction organ motion variations and adapt the treatment accordingly, however at the cost of extra imaging dose to the patient.

With the aim of providing a treatment plan with improved robustness to such variations, four-dimensional magnetic resonance imaging (4DMRI) was recently made available to capture respiratory motion variability as a way to complement and support 4DCT [24–26]. MRI combines superior soft tissue contrast for better tumor visualization, fast dynamic sequences to provide motion description, and radiation-free imaging thus allowing long and repeated acquisitions [25,26].

Recently, several efforts have been dedicated to translating the information stored in the MRI to a synthetic CT which could be used for dose calculation [27,28]. As for the thoraco-abdominal site, bulk density assignment [29], atlas-based methods [30], probabilistic approaches [31] and deep learning strategies [32] were proposed, though none of them dealing with organ motion. Boye et al. [33] instead, proposed a method to generate a virtual respiratory-correlated 4DCT dataset by applying the respiratory motion captured by a 4DMRI on an acquired reference static 3D CT using deformable image registration (DIR) for proton therapy of liver and pancreas tumors [34,35]. A similar approach has been recently proposed and validated by Meschini et al. [36] for patients with abdominal tumors treated with CIRT at CNAO, demonstrating the potential use of the virtual 4DCT as a radiation-free approach to capture organ motion variations in this peculiar treatment.

A limitation of the virtual 4DCT approach adopted at CNAO [36], consists in the limited field of view (FOV) of the acquired 4DMRI (i.e. 12.5 cm in the right-left direction). This is due to MRI constraints, which prevent the acquisition of 3D data with adequate temporal and spatial resolution, and to the need to adopt 4DMRI image-based retrospective sorting [37] instead of ad-hoc MR sequences which are not always available in clinical scanners [38]. To overcome the issue, motion modelling techniques can be adopted [39], with those based on the propagation of the acquired motion outside the FOV being the most straightforward [40,41]. Among these, Paganelli et al. [40] extended the FOV in case of 2D orthogonal fast MRI slices by propagating the motion field derived by DIR between a reference static image and the corresponding 2D slices, whereas Ziegler et al. [41] derived the information outside of a truncated CBCT by modulating the motion field derived by mapping a planning CT on the daily CBCT.

In this study, we extended the 4DMRI FOV to the entire involved patient anatomy [40,41], in order to evaluate the use of the virtual 4DCT in CIRT of the abdominal site when considering complex beam geometries, as implemented in the clinic. The proposed approach was validated relying on an anthropomorphic computational phantom, by simulating realistic inter- and intra-fractional organ motion variations. The method was then retrospectively applied to eight patient cases with abdominal tumors, treated with gated CIRT at CNAO. Organ motion variations as described in the planning and the virtual 4DCTs were therefore quantified in a clinical scenario for CIRT in terms of both geometric and dosimetric changes, by studying tumor displacement and evaluating the impact of motion on the treatment plan, respectively.

2 Material and methods

2.1 Patient dataset

In this study, we considered data from six pancreas and two liver patients treated at CNAO with CIRT using the respiratory gating technique, i.e. by synchronizing dose delivery with the end-exhale phase as detected through an external surrogate signal [7,15,42]. Informed consent for data acquisition was obtained from the patients according to institutional standards. Patients were immobilized using customized pillows (MOLDCARE Cushion, QFix Avondale PA, USA) and non-perforated body thermoplastic masks (Klarity Medical Products, USA), implying a moderate abdominal compression and reduced amplitude of the diaphragm excursion. The same immobilization setup was used for both CT and MRI scans and treatment delivery.

The 4DCT scans were acquired during free breathing with a Siemens SOMATOM Sensation Open CT (Siemens Healthcare GmbH, Germany) scanner with resolution of $0.98 \times 0.98 \times 2$ mm. Image acquisition was coupled to a pressure sensor (AZ-733V system, Anzai Medical Co. Ltd., Japan) placed between the patient body and the solid mask. Images were retrospectively reconstructed using the external respiratory surrogate signal at the following respiratory phases: end-exhale (0%EX), 30%-exhale (30%EX), 30%-inhale (30%IN), end-inhale (100%IN). In the same day of the planning 4DCT, multi-slice MRI sagittal images of the abdomen were acquired during free breathing with the T2/T1-weighted balanced steady-state free precession sequence (TrueFISP) using a 3 T scanner (Magnetom Verio, Siemens Healthcare GmbH, Germany). The imaged volume consisted of 25 sagittal slices, including a field of view (FOV) limited to 12.5 cm in the right-left direction (Fig. 1); for each slice 30 frames were acquired (TR/TE: 228.07 ms/1.5 ms; flip angle: 33°; scan matrix: 256×256 pixels with spacing of 1.33×1.33 mm; slice thickness of 5 mm; acquisition time: 310 ms/slice with 25 slices $\times$ 30 frames; k-space percentage sampling: 65%; acceleration factor: 2 with a generalized auto-calibrating partially parallel acquisition using 16 auto-calibration lines). The 4DMRI was retrospectively reconstructed by means of an algorithm based on clustering and image-based multidimensional surrogates [37]. The 0%EX, 30%EX, 30%IN and 100%IN respiratory phases were considered in the 4DMRI as in the 4DCT.

In the considered patient group, IMPT clinical plans were defined for each patient in supine setup comprising one or two lateral beams and one antero-posterior beam. Carbon ion prescription RBE-weighted doses ranged between 55.2 and 57.6 Gy(RBE) in 12 fractions. The internal gross tumor volume (IGTV) was defined as the union of the gross tumor volumes (GTV), as described in the four 4DCT phases. For liver tumors, the clinical target volume (CTV) was derived as an isotropic expansion of the IGTV, then subject to clinical evaluation to ensure the inclusion of microscopic tumor infiltrations. For pancreatic tumors, the CTV was defined as the GTV with a 5 mm margin including the locoregional elective lymph nodes and neuroplexus region [7]. The planning target volume (PTV) was derived by adding 3–5 mm margin to the CTV, depending on target location and organs at risk proximity [43]. Plans were optimized with the RayStation treatment planning system (TPS) (RaySearch Laboratories, Sweden). Treatment planning workflow for moving target consists in plan optimization on the 0%EX CT and recalculation on the expected gating window phases (i.e. 30%EX, 30%IN) to evaluate the dosimetric impact of residual motion [42]. For clinical approval, target dose coverage and organs at risk (OARs) limits must be guaranteed in the three computed dose distributions. Quantifications about the unexpected scenario of plan delivery outside the gating window is provided by the plan recalculation on the 100%IN CT.

2.2 Virtual 4DCT generation with extended FOV

The virtual 4DCT was generated by deforming a reference CT in order to match the anatomy depicted in the 4DMRI within its FOV and to obtain physically plausible deformation outside of the 4DMRI FOV.

Deformable image registration (DIR) was performed to obtain the deformation vector fields (DVFs) as defined within the 4DMRI FOV. The baseline DVF was obtained by registering the reference CT to the 0%EX MRI, whereas breathing motion was described by DVFs calculated by registering the 0%EX MRI to all other 4DMRI respiratory phases, following the approach proposed by Meschini et al. [36]. The parameters related to inter- and intra-modality DIR are reported in Supplementary Materials S1 [44–46].

A method to extrapolate DVF information outside of the 4DMRI FOV was applied. Specifically, each DVF was extended by: (i) propagating the DVF at the boundary of the FOV (i.e. in correspondence to the two extreme sagittal slices) to the surrounding voxels outside of the FOV [40], (ii) multiplying the propagated DVF in each voxel by a decaying function of the form 1/(1+0.1*d) [41], where d is the distance of the voxel to the closest point within the FOV, expressed in millimeters. This modulation of the DVF was aimed at limiting the impact of motion misestimations outside of the 4DMRI FOV and producing limited discontinuities in the deformed images. Additionally, the DVFs were set to zero outside of the abdomen [33,36], as the spine and the ribcage were assumed to be steady in patients wearing semirigid immobilization masks.

The reference CT was deformed according to the extended baseline DVF, thus obtaining the virtual 0%EX CT. Then, the other respiratory phases of the virtual 4DCT were generated by deforming the virtual 0%EX CT according to the extended DVFs derived from 4DMRI breathing motion.

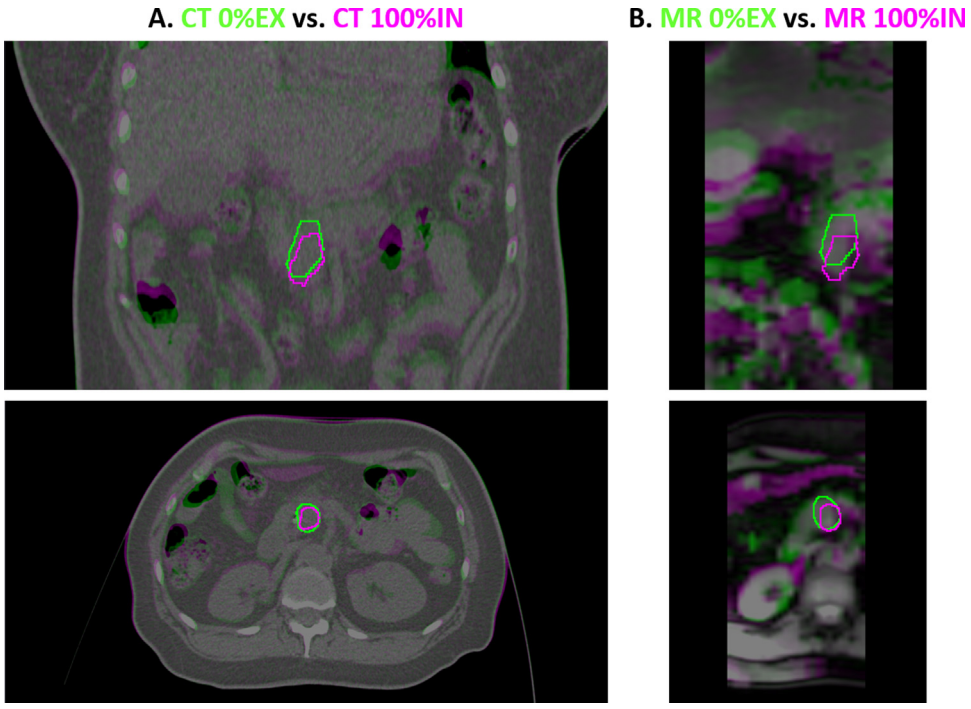

Figure 1. Coronal and axial views of the end-exhale (green) and the end-inhale (violet) respiratory phases in the 4DCT (A) and 4DMRI (B), with the corresponding GTV contours.

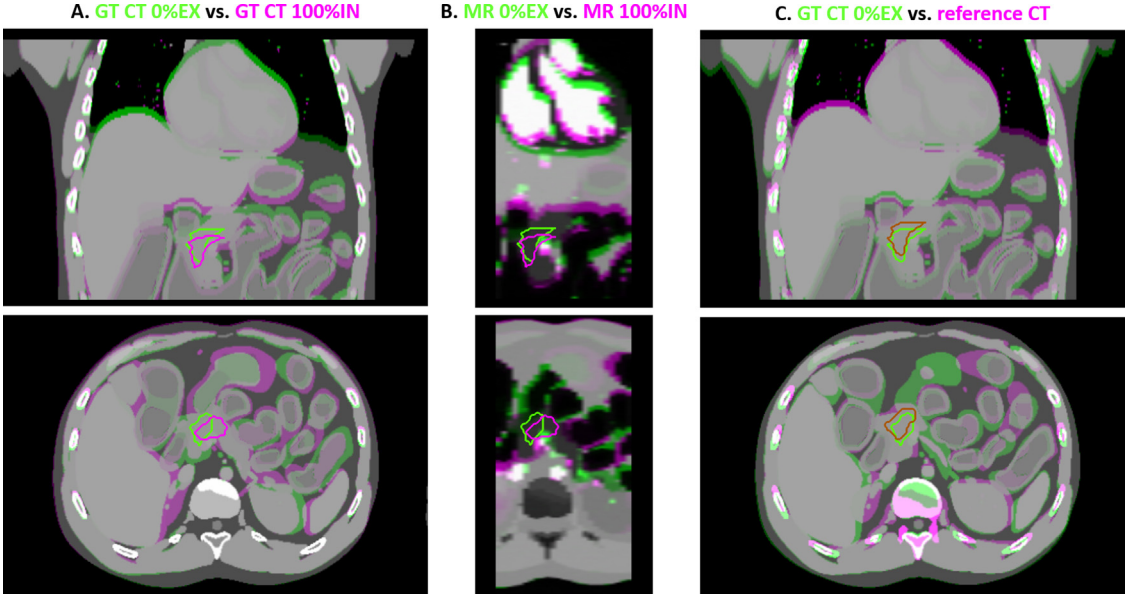

Figure 2. Overlay between the end-exhale (green image and target contour) and end-inhale (violet image and target contour) respiratory phases of the ground truth 4D XCAT (A) and the CoMBAT phantom (B). In panel C, overlay between the ground truth end-exhale CT (green image and contour) and the reference CT (violet image, brown contour) generated through a rigid baseline variation.

2.3 Phantom validation

The method was validated on a digital anthropomorphic phantom. Specifically, a 4D XCAT phantom [47] of the abdomen was generated, exhibiting a range of motion of the diaphragm (superior–inferior direction) and of the chest wall (anterior–posterior direction) of 8.8 mm and 3.0 mm, respectively (Fig. 2A). A pseudo-clinical target was defined

by copying the target of a pancreas patient on the phantom planning CT, and manually adjusting the contours on the phantom anatomy. The resulting target motion range was 6.1 mm, which is comparable to literature values for patients treated with gated CIRT [42]. A 4DCT was obtained with the 4 respiratory phases used for treatment planning on patients (i.e. 0%EX, 30%EX, 30%IN and 100%IN). The corresponding 4DMRI was then derived by means of the 4D CoMBAT digital phantom [48] (Fig. 2B). The reference 3D CT for treatment planning and virtual 4DCT generation was obtained by simulating a rigid baseline variation with respect to the end-exhale respiratory phase (Fig. 2C). In the considered patient group, a 6 mm median variation of the tumor baseline position was measured, thus an equivalent change was applied for the reference CT generation in the phantom study. Imaging parameters reported in Section 2.2 were applied for both CT and MRI phantom simulations.

A carbon ion treatment plan was optimized on the reference CT with the RayStation TPS. According to the protocol for pancreas patients treated with CIRT at CNAO, an RBE-weighted dose of 57.6 Gy(RBE) was prescribed and the plan was defined with an anterior and two lateral opposite beams. The dose distribution was recalculated on both the ground truth (GT) 4DCT and on the virtual 4DCT. The ground truth motion was assessed through DIR between GT 4DCT phases, yielding to the estimation of GT DVFs. The accuracy of the method was evaluated by computing:

- the target center of mass (COM) distance between corresponding phases of the virtual and GT 4DCTs, thus quantifying the geometrical estimation error within the 4DMRI FOV; this was compared against the motion described in the GT 4DCT, as quantified by the target COM distance between the GT respiratory phases and the reference CT;
- the mean difference between GT and virtual CT DVFs outside of the 4DMRI FOV, obtained by (i) masking the DVFs, (ii) computing the 3D (norm) difference, (iii) calculating the mean value over the evaluated voxels. This metric represented the geometrical estimation error outside of the 4DMRI FOV; it was compared against the mean GT DVFs amplitude;
- the difference of relevant dose-volume histogram (DVH) metrics such as the dose to the 5% ($D_{5\%}$) and 95% ($D_{95\%}$) of the target volume, computed according to the formula:

$$\Delta Dn\%|_{XY} = \frac{D_{n\%X} - D_{n\%Y}}{D_{n\%Y}}$$

where $n = 5\%$ or 95%, whereas X and Y are either vCT, GT or Plan, referring to the dose computed on the virtual, GT or planning CT, respectively. Specifically, the method estimation error was quantified by $\Delta Dn\%|_{vCT,GT}$, whereas the motion impact was measured by $\Delta Dn\%|_{GT,plan}$.

2.4 Clinical data analysis

In the considered patient group, the 0%EX CT was used both to optimize treatment plan and as reference to generate the virtual 4DCT. The patient-specific DIR validation is reported in Supplementary Materials S2. The clinical treatment plans were re-optimized and recomputed on all respiratory phases of the planning and virtual 4DCTs in the RayStation TPS. A ground truth was not available in the patients' cases and the virtual 4DCT allowed to evaluate organ motion variability and its impact on the clinical dose distributions. The inter-fractional variations and motion variabilities described in the virtual 4DCT with respect to the planning 4DCT were quantified by:

- the displacement of the target position between the CT and MRI scans at end-exhale (i.e. baseline variation), computed as the tumor COM distance between the virtual and planning 0%EX CTs;
- the tumor range of motion (ROM) in the two datasets (i.e. planning and virtual 4DCTs), computed as the distance of tumor COM in the 0%EX and the 100%IN;
- the tumor $\Delta Dn\%|_{vCT,plan}$ and $\Delta Dn\%|_{CT,plan}$ with n = 5% and 95%, as computed considering all phases of virtual and planning 4DCTs, respectively.
- the $\Delta D2\%|_{vCT,plan}$ and $\Delta D2\%|_{CT,plan}$ to OARs in the beams path. Specifically, for pancreas patients, OARs related to the risk of gastrointestinal (GI) ulcer were considered, given that similar maximum dose values were adopted (RBE-weighted dose < 48 Gy(RBE) for colon; RBE-weighted dose < 43 Gy(RBE) for stomach and small bowels).

3 Results

3.1 Phantom validation

Despite a target displacement ranging from 6.0 to 12.1 mm between the reference CT and the virtual 4DCT (COM motion in Table 1), the geometrical accuracy of the virtual 4DCT in correspondence to the target was below 1 mm, as seen in the target COM distance between virtual and GT 4DCT phases (COM error in Table 1). The geometrical estimation error is larger outside of the 4DMRI FOV (up to 4.5 mm at 0%EX), and comparable to the GT motion, as estimated from the GT and virtual 4DCTs DVFs (Table 1).

Both the motion and the estimation error had a negligible impact on $D_{5\%}$, indeed $\Delta D5\%|_{vCT,plan}$ and the $\Delta D5\%|_{vCT,GT}$ presented values below 1% (Table 2). The impact of motion was more evident on $D_{95\%}$, with $\Delta D95\%|_{GT,plan}$ values between −22.0% and −90.3%, however, the corresponding estimation error was ≤2.2% (Table 2). Fig. 3A shows the dose distribution recalculated on the 100%IN GT CT, which is

Table 1
Geometrical estimation accuracy: error on target COM position (COM error) computed by comparing the virtual and GT 4DCT phases; tumor motion between reference and GT CTs (COM motion); difference between DVF as estimated from the GT 4DCT and from the virtual 4DCT method (DVF error); mean GT DVF amplitude (DVF motion).

Respiratory phase	COM error [mm]	COM motion [mm]	DVF error [mm]	DVF motion [mm]
0%EX	0.7	6.0	4.5	4.9
30%EX	0.4	7.6	0.8	0.9
30%IN	0.8	8.2	1.2	1.4
100%IN	0.8	12.1	2.8	3.1

Table 2
Dosimetric estimation accuracy: $D_{5\%}$ and $D_{95\%}$ difference between the doses computed on the virtual and the GT 4DCT (second and fourth columns) measuring the error introduced by the virtual 4DCT; $D_{5\%}$ and $D_{95\%}$ difference between the dose computed on the GT 4DCT and the planned dose, quantifying the impact of the motion on the dose distribution.

Respiratory phase	$\Delta D5\%\|_{vCT,GT}$	$\Delta D5\%\|_{GT,plan}$	$\Delta D95\%\|_{vCT,GT}$	$\Delta D95\%\|_{GT,plan}$
0%EX	0.0%	−0.2%	1.6%	−22.0%
30%EX	0.0%	−0.2%	1.3%	−52.0%
30%IN	−0.2%	0.0%	2.2%	−53.0%
100%IN	−0.2%	0.0%	0.0%	−90.3%

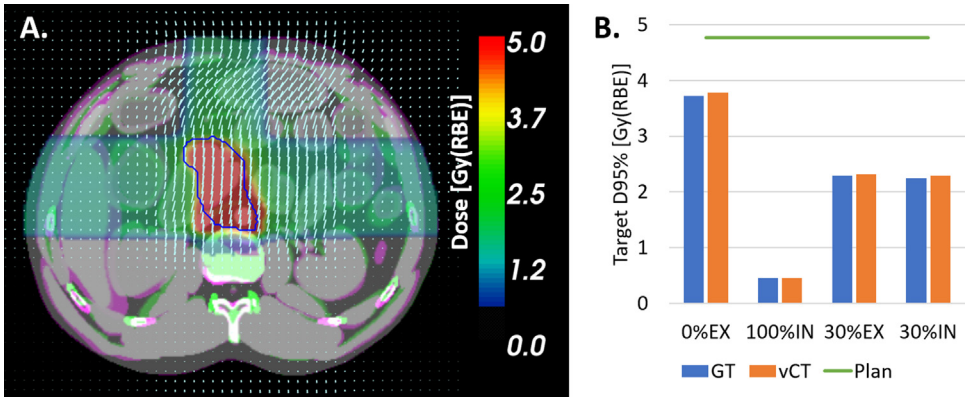

Figure 3. A. Overlay between GT (violet) and virtual (green) 100%IN CTs, with the extended DVF (light blue arrows) before setting it to zero outside of the abdomen. The RBE-weighted dose distribution is displayed as fusion map and the target is represented by the blue contour. B. Bar plot of the target $D_{95\%}$ (RBE-weighted fraction dose) as computed on the virtual (vCT) and GT 4DCTs, against the planned $D_{95\%}$ (green line).

severely degraded, as confirmed by the $D_{95\%}$ decrease shown in Fig. 3B.

3.2 Patient analysis

The variation of the baseline tumor position between the virtual and the planning 0%EX CTs presented a 6.0 mm median value and 4.9 mm interquartile range (values for each patient are displayed in Fig. 4). Different ROM between the two datasets were recorded (Fig. 4): in 5 out of 8 patients, the virtual 4DCTs described a larger ROM with respect to the planning 4DCT. For patients with baseline variations larger than 5 mm, $\Delta D95\%|_{vCT,plan}$ resulted in absolute variations higher than 10% at 0%EX.

Fig. 5 shows two example patient cases: the dose distribution as computed on the 0%EX of the planning and virtual 4DCTs for P2 (Fig. 5A and B, respectively), where the target miss is noticeable ($\Delta D95\%|_{vCT,plan} = -49.8\%$), and for P8 (Fig. 5C and D), who presented the largest baseline variation (11.4 mm). It can be noticed that inter-fractional variations described in the virtual 4DCT turned into dose variations to the target.

As for the dosimetric impact of inter-fractional breathing variability, the tumor $\Delta D5\%|_{vCT,plan}$ and $\Delta D5\%|_{CT,plan}$ remained below 2.5% for the 30%EX/30%IN (Fig. 6A) and 100%IN (Fig. 6B) phases. Differently, $\Delta D95\%|_{vCT,plan}$ presented slightly lower median values with respect to $\Delta D95\%|_{CT,plan}$ (−3.8% vs. −1.9% for 30%EX/IN, −19.7% vs. −16.2% for 100%IN), as noticeable in Fig. 6C and

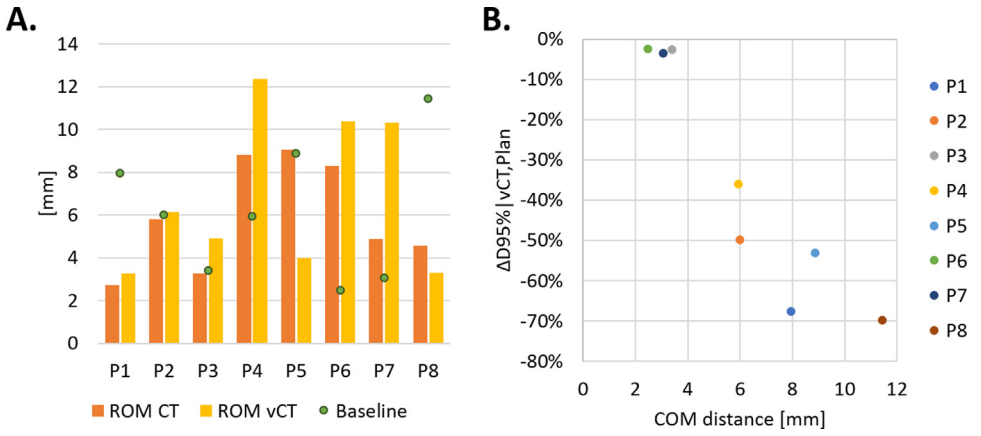

Figure 4. (A) Barplot of target range of motion (ROM) in the virtual (vCT) and planning (CT) 4DCTs for each patient, with the corresponding values of baseline variations (green dots); (B) Tumor $\Delta D95\%|_{vCT,plan}$ as computed at the 0%EX against the corresponding baseline variation.

D. For OARs, analysis was carried out in terms of relative difference. Out of 21 structures, 7 OARs presented $\Delta D2\%|_{vCT,plan}$ >5% at 0%EX. The mean (standard deviation) $\Delta D2\%|_{vCT,plan}$ (considering its absolute values) was 3.2% (3.8%) in the 30%EX and 30%IN phases, and 27.3% (74.7%) in the 100%IN. At 100%IN, $\Delta D2\%|_{vCT,plan}$ presented larger values than $\Delta D2\%|_{CT,plan}$ in 11 structures.

4 Discussion

Capturing possible motion variations along the treatment course is fundamental to determine when adaptive replanning is appropriate. When the acquisition of daily 4D cone-beam CT (CBCT) [21] is not feasible, the use of repeated 4DCT acquisition, usually on a weekly basis [10], is strongly suggested. Virtual 4DCT from 4DMRI offers a radiation-free method to capture inter- and intra-fractional motion variability as a supportive tool for treatment planning [33,36]. In this study, we were able to evaluate the use of virtual 4DCT with extended FOV in the investigation of a clinical scenario for gated CIRT of abdominal tumors.

The method was initially validated on a digital phantom by simulating a rigid baseline variation with respect to the reference end-exhale respiratory phase, as measured in the patients' cohort. Within the 4DMRI FOV, a geometrical accuracy comparable to DIR accuracy is expected: DIR error was indeed quantified with a patient-specific approach [44] (Supplementary Materials), resulting in a median error lower than 2 mm. In this study, geometrical accuracy was found to be submillimetric in correspondence to the target, whereas an error up to 4.5 mm was quantified outside of the FOV. This result suggests the underestimation of motion outside of the 4DMRI FOV, due to the strong modulation of the propagated DVF [41]. Nevertheless, the method was able to compensate for large variations between the GT and the reference CT (absolute $\Delta D95\%|_{GT,plan}$ >22%), and estimation error on dose metrics was lower than 2.2% (maximum $\Delta D95\%|_{vCT,GT}$). Therefore, the limited impact of the geometrical inaccuracy on the estimated dose distribution suggests that the use of virtual 4DCT from 4DMRI with extended FOV is feasible in CIRT planning of the abdominal site.

In the analyzed patient group, the virtual 4DCTs were compared with the acquired planning 4DCT datasets. Differently from Meschini et al. [36], the availability of extended FOV CTs allowed the evaluation of clinical plans, i.e. actual beam geometry and particle fluence. The use of thermoplastic immobilization masks reduces the breathing motion amplitude, thus also limiting the geometrical inaccuracy of the virtual 4DCT outside of the 4DMRI FOV. As in the phantom simulation, a limited impact of geometrical inaccuracy on the dose distribution calculated on the estimated virtual 4DCT is expected, due to robust beam geometry configuration and reduced particle fluence to anticipate beam paths modifications in the regions of tissue density heterogeneities (e.g. air filling of the bowels, moving ribs).

In the collected patients, 4DMRI images were acquired the same day of the planning 4DCT. Despite being acquired in the same day, the repositioning of the patient on the MRI couch introduces changes comparable to inter-fractional ones. Therefore, the generated virtual 4DCT provided indications on possible inter-fractional variations with respect to the planning 4DCT for targets subject to organ motion in the abdominal region. As such, the comparison at the 0%EX phase showed that significant geometrical baseline variations were observed in the majority of the cases, which translated to target $D_{95\%}$ dosimetric variations of more than 10% for baseline changes larger than 5 mm (Fig. 4B). Relevant differences were also observed in $D_{2\%}$ in 7 out of 21 cases for the involved abdominal OARs. Both situations may lead to treatment adaptations and replanning in the current clinical workflow.

The virtual 4DCT was also able to capture motion variability at different respiratory phases. Median variations higher than 10% in the target $D_{95\%}$ and GI OARs $D_{2\%}$

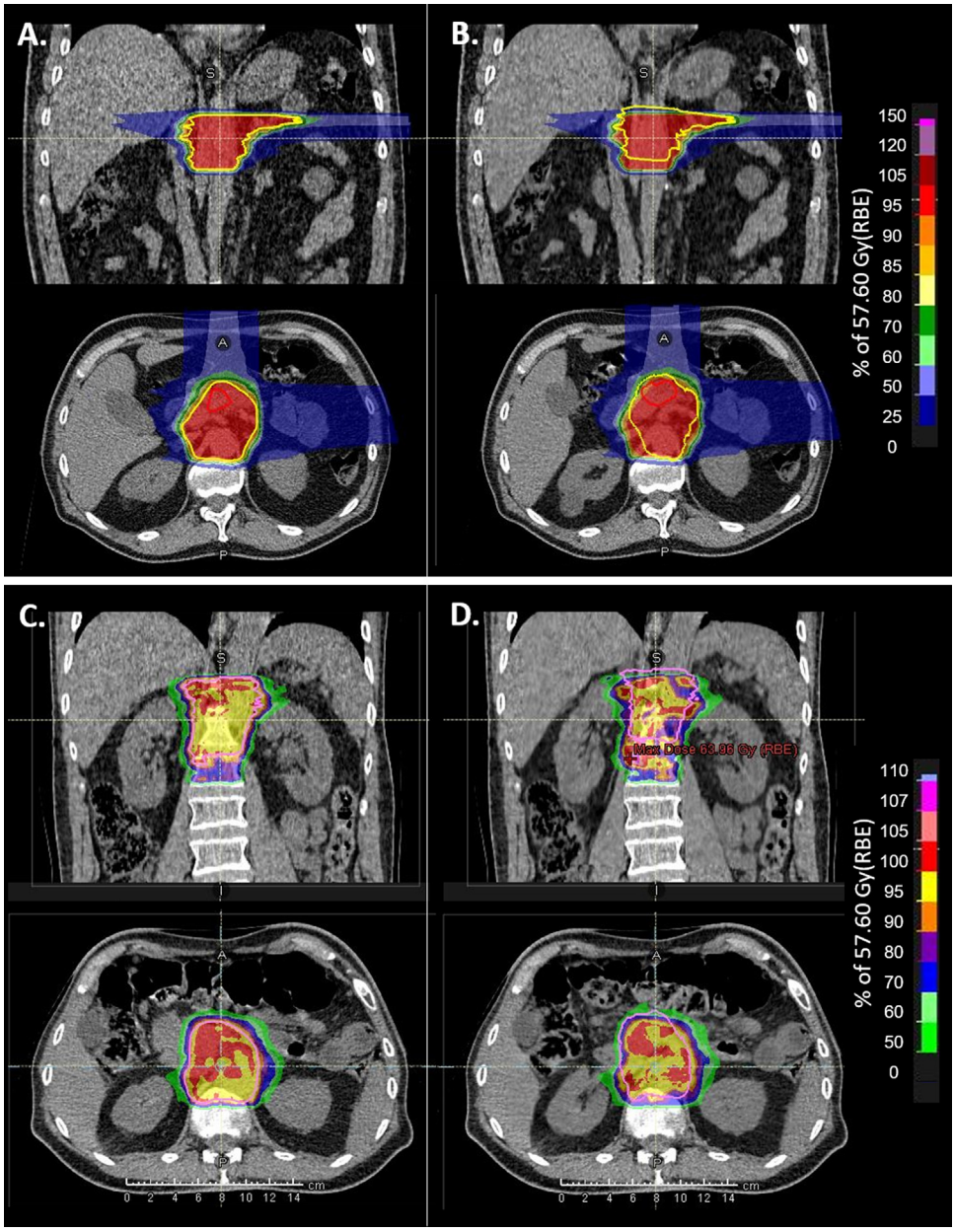

Figure 5. Planned dose distribution on the 0%EX CT (A. and C.) and dose recalculation on the 0%EX virtual CT (B. and D.) for P2 and P8, where the tumor is represented by the yellow and pink contour, respectively. In C. and D., the visualized dose range comprises high dose values in order to highlight dose distribution differences in the target, consequently the beam paths are not displayed.

were quantified at the 100%IN phase (Fig. 4D), because different motion between planning and virtual 4DCTs led to degraded target dose coverage. Differently, close to end-exhale (30%EX/30%IN phases), only limited variations of relevant dose metrics were found for both tumor and OARs, confirming that the tumor coverage and dosimetric safety for OARs were guaranteed thanks to a conservative approach against residual motion within the expected gating window.

Main limitations in this study are connected to the method for 4DMRI FOV extension. The modulation of the propagated DVF outside of the FOV is effective in limiting anatomical discontinuities and permits an effective dosimetric analysis, but it underestimates motion, thus alternative motion modelling techniques [39] or ad-hoc imaging acquisition to directly derive extended FOV 4DMRI [38] need to be considered. Moreover, relevant anatomical changes (e.g. variability in bowel filling and positioning) for the organs outside of the

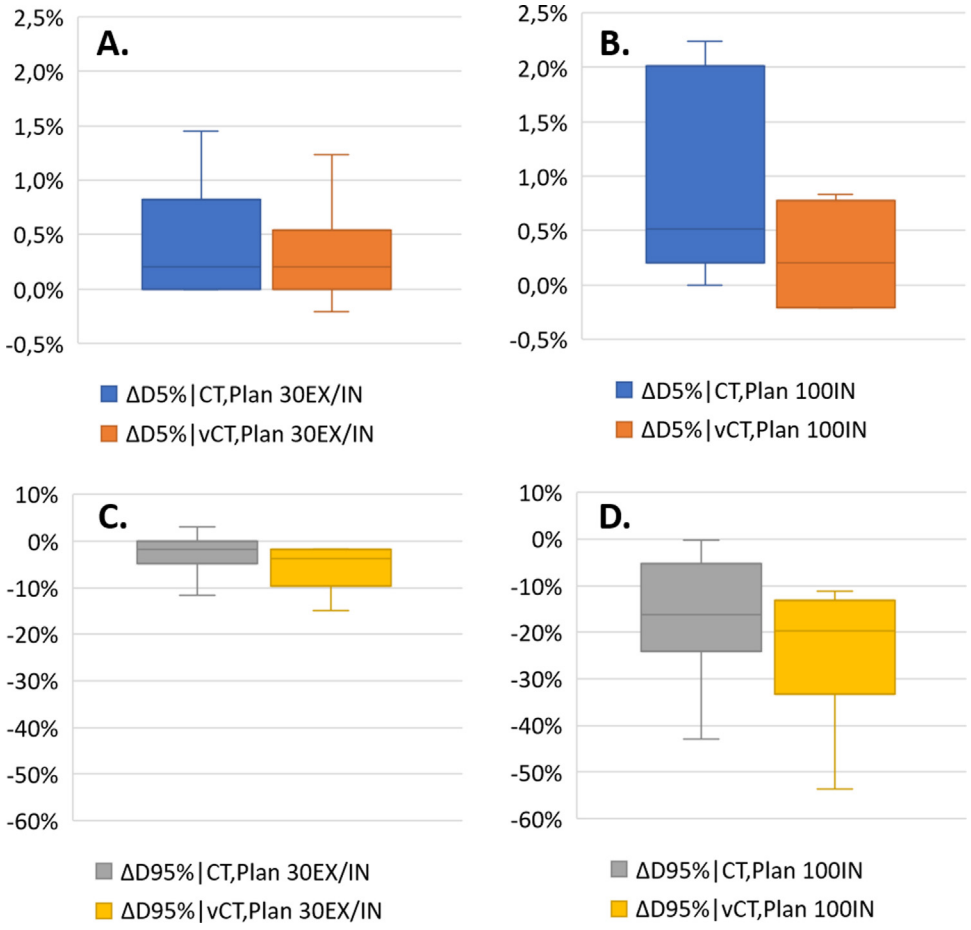

Figure 6. Tumor dose differences for $D_{5\%}$ and $D_{95\%}$ as computed considering 30%EX and 30%IN (panel A. and C., respectively) and considering the 100%IN (panel B. and D.) of virtual (vCT) and planning (CT) 4DCTs.

4DMRI FOV may occur, which would be neglected in the virtual 4DCT generation, causing variations in the dose distributions. Acquiring a 3D MRI comprising the entire involved FOV at the same time of the 4DMRI acquisition represents a simple solution to detect possible severe anatomical variation and to update the reference anatomy.

In the future, the virtual 4DCT will be investigated as a tool to evaluate intra-fractional variations, by applying the described method on repeated 4DMRI acquired on each patient within the same imaging session along the treatment course, also extending the analysis to a larger number of patient cases. Additionally, the use of the virtual 4DCT for 4D robust treatment planning [49,50] could be investigated. For the considered patient group, only clinical plans in supine setup were investigated. At CNAO, in the clinical workflow for abdominal tumor treatment, a proper combination of supine and prone setup treatment fractions is usually implemented, in order to reduce OARs dose. The acquisition of 4DMRI in prone setup is technically feasible and the generation of corresponding virtual 4DCTs will be explored as a future development.

5 Conclusions

In this study the generation of extended FOV virtual 4DCTs from 4DMRI was proved to be feasible and accurate and could be used to support the clinical workflow for studying organ motion occurring during CIRT of abdominal tumors at no costs in terms of imaging radiation to the patient.

Conflict of interests

The authors declare that they have no known competing financial interests or personal relationships that could have appeared to influence the work reported in this paper.

Appendix A Supplementary data

Supplementary data associated with this article can be found, in the online version, at https://doi.org/10.1016/j.zemedi.2020.08.005.

References

[1] Rackwitz T, Debus J. Clinical applications of proton and carbon ion therapy. Semin Oncol 2019;46:226–32.

[2] Durante M, Orecchia R, Loeffler JS. Charged-particle therapy in cancer: clinical uses and future perspectives. Nat Rev Clin Oncol 2017;14:483–95.

[3] Kawashiro S, Yamada S, Okamoto M, Ohno T, Nakano T, Shinoto M, et al. Clinical Investigation Multi-institutional Study of Carbon-ion Radiotherapy for Locally Advanced Pancreatic Cancer: Japan Carbon-ion Radiation Oncology Study Group (J-CROS) study 1403 pancreas radiation oncology. Int J Radiat Oncol Biol Phys 2018;101(5):1212–21.

[4] Shibuya K, Ohno T, Terashima K, Toyama S, Yasuda S, Tsuji H, et al. Short-course carbon-ion radiotherapy for hepatocellular carcinoma: a multi-institutional retrospective study. Liver Int 2018;38(12):2239–47.

[5] Dell'oro M, Short M, Wilson P, Bezak E. Clinical limitations of photon, proton and carbon ion therapy for pancreatic cancer. Cancers 2020;12:163.

[6] Spychalski P, Kobiela J, Antoszewska M, Błażyńska-Spychalska A, Jereczek-Fossa BA, Høyer M, et al. Patient specific outcomes of charged particle therapy for hepatocellular carcinoma – a systematic review and quantitative analysis. Radiother Oncol 2019;132:127–34.

[7] Vitolo V, Cobianchi L, Brugnatelli S, Barcellini A, Peloso A, Facoetti A, et al. Preoperative chemotherapy and carbon ions therapy for treatment of resectable and borderline resectable pancreatic adenocarcinoma: a prospective, phase II, multicentre, single-arm study. BMC Cancer 2019;19(1):1–7.

[8] Mori S, Knopf A, Umegaki K. Motion management in particle therapy. Med Phys 2018;45(11):e994–1010.

[9] Knopf A-C, Boye D, Lomax A, Mori S. Adequate margin definition for scanned particle therapy in the incidence of intrafractional motion. Phys Med Biol 2013;58(17):6079–94.

[10] Chang JY, Zhang X, Knopf A, Li H, Mori S, Dong L, et al. Consensus Guidelines for Implementing Pencil-Beam Scanning Proton Therapy for Thoracic Malignancies on Behalf of the PTCOG thoracic and lymphoma subcommittee. Int J Radiat Oncol Biol Phys 2017;99:41–50.

[11] Mori S, Zenklusen S, Inaniwa T, Furukawa T, Imada H, Shirai T, et al. Conformity and robustness of gated rescanned carbon ion pencil beam scanning of liver tumors at NIRS. Radiother Oncol 2014;111(3):431–6.

[12] Bert C, Durante M. Motion in radiotherapy: particle therapy. Phys Med Biol 2011;56(16):R113–44.

[13] Rosu M, Hugo GD. Advances in 4D radiation therapy for managing respiration: Part II – 4D treatment planning. Z Med Phys 2012;22(4):272–80.

[14] Pfeiler T, Bäumer C, Engwall E, Geismar D, Spaan B, Timmermann B. Experimental validation of a 4D dose calculation routine for pencil beam scanning proton therapy. Z Med Phys 2018;28(2):121–33.

[15] Ciocca M, Mirandola A, Molinelli S, Russo S, Mastella E, Vai A, et al. Commissioning of the 4-D treatment delivery system for organ motion management in synchrotron-based scanning ion beams. Phys Med 2016;32(12):1667–71.

[16] Keall PJ, Mageras GS, Balter JM, Emery RS, Forster KM, Jiang SB, et al. The management of respiratory motion in radiation oncology report of AAPM Task Group 76. Med Phys 2006;33(10):3874–900.

[17] Batista V, Richter D, Chaudhri N, Naumann P, Herfarth K, Jäkel O. Significance of intra-fractional motion for pancreatic patients treated with charged particles. Radiat Oncol 2018;13(1):120.

[18] Fiorina E, Ferrero V, Pennazio F, Baroni G, Battistoni G, Belcari N, et al. Monte Carlo simulation tool for online treatment monitoring in hadrontherapy with in-beam PET: a patient study. Phys Med 2018;51:71–80.

[19] Dhont J, Vandemeulebroucke J, Burghelea M, Poels K, Depuydt T, Van Den Begin R, et al. The long- and short term variability of breathing induced tumor motion in lung and liver over the course of a radiotherapy treatment. Radiother Oncol 2018;126:339–46.

[20] Landry G, Hua C. Current state and future applications of radiological image guidance for particle therapy. Med Phys 2018;45:e1086–95.

[21] Niepel K, Kamp F, Kurz C, Hansen D, Rit S, Neppl S, et al. Feasibility of 4DCBCT-based proton dose calculation: an ex vivo porcine lung phantom study. Z Med Phys 2019;29:249–61.

[22] Kurz C, Dedes G, Resch A, Reiner M, Ganswindt U, Nijhuis R, et al. Comparing cone-beam CT intensity correction methods for dose recalculation in adaptive intensity-modulated photon and proton therapy for head and neck cancer. Acta Oncol 2015;54(9):1651–7.

[23] Fotina I, Hopfgartner J, Stock M, Steininger T, Lütgendorf-Caucig C, Georg D. Feasibility of CBCT-based dose calculation: comparative analysis of HU adjustment techniques. Radiother Oncol 2012;104:249–56.

[24] Fontana G, Riboldi M, Gianoli C, Chirvase CI, Villa G, Paganelli C, et al. MRI quantification of pancreas motion as a function of patient setup for particle therapy – a preliminary study. J Appl Clin Med Phys 2016;17(5):60–75.

[25] Paganelli C, Whelan B, Peroni M, Summers P, Fast M, Van De Lindt T, et al. MRI-guidance for motion management in external beam radiotherapy: current status and future challenges. Phys Med Biol 2018;63, 22TR03.

[26] Stemkens B, Paulson ES, Tijssen RHN. Nuts and bolts of 4D-MRI for radiotherapy. Phys Med Biol 2018;63(21), 21TR01.

[27] Johnstone E, Wyatt JJ, Henry AM, Short S, Sebag-Montefiore D, Murray L, et al. Systematic review of synthetic computed tomography generation methodologies for use in magnetic resonance imaging-only radiation therapy. Int J Radiat Oncol Biol Phys 2018;100:199–217.

[28] Owrangi A, Greer P, Glide-Hurst C. MRI-only treatment planning: benefits and challenges. Phys Med Biol 2018;63, 05TR01.

[29] Freedman JN, Bainbridge HE, Nill S, Collins DJ, Kachelrieß M, Leach MO, et al. Synthetic 4D-CT of the thorax for treatment plan adaptation on MR-guided radiotherapy systems. Phys Med Biol 2019;64(11):115005.

[30] Guerreiro F, Koivula L, Seravalli E, Janssens GO, Maduro JH, Brouwer CL, et al. Feasibility of MRI-only photon and proton dose calculations for pediatric patients with abdominal tumors. Phys Med Biol 2019;64(5), 055010.

[31] Bredfeldt JS, Liu L, Feng M, Cao Y, Balter JM, Synthetic CT. for MRI-based liver stereotactic body radiotherapy treatment planning. Phys Med Biol 2017;62:2922–34.

[32] Liu Y, Lei Y, Wang Y, Wang T, Ren L, Lin L, et al. MRI-based treatment planning for proton radiotherapy: dosimetric validation of a deep learning-based liver synthetic CT generation method. Phys Med Biol 2019;64:145015.

[33] Boye D, Lomax T, Knopf A. Mapping motion from 4D-MRI to 3D-CT for use in 4D dose calculations: a technical feasibility study. Med Phys 2013;40(6.).

[34] Bernatowicz K, Peroni M, Perrin R, Weber DC, Lomax A. Four-dimensional dose reconstruction for scanned proton therapy using liver 4DCT-MRI. Int J Radiat Oncol Biol Phys 2016;95(1):216–23.

[35] Dolde K, Naumann P, Dávid C, Kachelriess M, Lomax AJ, Weber DC, et al. Comparing the effectiveness and efficiency of various gating approaches for PBS proton therapy of pancreatic cancer using 4D-MRI datasets. Phys Med Biol 2019;64, 085011.

[36] Meschini G, Vai A, Paganelli C, Molinelli S, Fontana G, Pella A, et al. Virtual 4DCT from 4DMRI for the management of respiratory motion in carbon ion therapy of abdominal tumors. Med Phys 2019.

[37] Meschini G, Paganelli C, Gianoli C, Summers P, Bellomi M, Baroni G, et al. A clustering approach to 4D MRI retrospective sorting for the investigation of different surrogates. Phys Med 2019;58:107–13.

[38] Deng Z, Pang J, Yang W, Yue Y, Sharif B, Tuli R, et al. 4D MRI using 3D radial sampling with respiratory self-gating to characterize temporal phase-resolved respiratory motion in the abdomen. Magn Reson Med 2016;75(4):1574–85.

[39] Paganelli C, Portoso S, Garau N, Meschini G, Via R, Buizza G, et al. Time-resolved volumetric MRI in MRI-guided radiotherapy: an in silico comparative analysis. Phys Med Biol 2019;64(18), 185013.

[40] Paganelli C, Lee D, Kipritidis J, Whelan B, Greer PB, Baroni G, et al. Feasibility study on 3D image reconstruction from 2D orthogonal

cine-MRI for MRI-guided radiotherapy. J Med Imaging Radiat Oncol 2018;62(3):389–400.
[41] Ziegler M, Nakamura M, Hirashima H, Ashida R, Yoshimura M, Bert C, et al. Accumulation of the delivered treatment dose in volumetric modulated arc therapy with breath-hold for pancreatic cancer patients based on daily cone beam computed tomography images with limited field-of-view. Med Phys 2019;46(7):2969–77.
[42] Meschini G, Seregni M, Pella A, Ciocca M, Fossati P, Valco F, et al. Evaluation of residual abdominal tumour motion in carbon ion gated treatments through respiratory motion modelling. Phys Med 2017;34:28–37.
[43] Meschini G, Seregni M, Molinelli S, Vai A, Phillips J, Sharp GC, et al. Validation of a model for physical dose variations in irregularly moving targets treated with carbon ion beams. Med Phys 2019;46:3663–73.
[44] Paganelli C, Meschini G, Molinelli S, Riboldi M, Baroni G. Patient-specific validation of deformable image registration in radiation therapy: overview and caveats. Med Phys 2018;45:e908.
[45] Brock KK, Mutic S, Li H, Kessler ML. Use of image registration and fusion algorithms and techniques in radiotherapy: Report of the AAPM Radiation Therapy Committee Task Group No. 132. Med Phys 2017;44:e43–76.
[46] Paganelli C, Peroni M, Riboldi M, Sharp GC, Ciardo D, Alterio D, et al. Scale invariant feature transform in adaptive radiation therapy: a tool for deformable image registration assessment and re-planning indication. Phys Med Biol 2013;58:287–99.
[47] Segars WP, Sturgeon G, Mendonca S, Grimes J, Tsui BM. 4D XCAT phantom for multimodality imaging research. Med Phys 2010;37:4902.
[48] Paganelli C, Summers P, Gianoli C, Bellomi M, Baroni G, Riboldi M. A tool for validating MRI-guided strategies: a digital breathing CT-MRI phantom of the abdominal site. Med Biol Eng Comput 2017;55:2001.
[49] Unkelbach J, Paganetti H. Robust proton treatment planning: physical and biological optimization. Semin Radiat Oncol 2018;28:88.
[50] Wolf M, Anderle K, Durante M, Graeff C. Robust treatment planning with 4D intensity modulated carbon ion therapy for multiple targets in stage IV non-small cell lung cancer. Phys Med Biol 2020, http://dx.doi.org/10.1088/1361-6560/aba1a3 (in press).